Supplementary Materials for

Entropy-driven stability of chiral single-walled carbon nanotubes

Yann Magnin, Hakim Amara, François Ducastelle, Annick Loiseau, Christophe Bichara*

*Corresponding author. Email: bichara@cinam.univ-mrs.fr

This PDF file includes:

Materials and Methods
Figs. S1 to S3
Caption for Movie S1
Caption for Data S1
Data S2
References

Other Supplementary Material for this manuscript includes the following:
(available at www.sciencemag.org/content/362/6411/212/suppl/DC1)

Movie S1 (.mp4)
Data S1 (.zip)

Methods

Density Functional Theory calculations
The first-principles code Quantum Espresso *(29)* employing density functional theory (DFT) within the projector-augmented wave (PAW) method *(30)* is used to calculate the formation energies of all possible (8, 4) edges. The generalized gradient approximation (GGA) *(31)* is employed for the exchange and correlation energy terms. We use a periodic cell allowing for 20 Å vacuum between the nanotubes to avoid interaction between neighboring supercells. Integrations over the Brillouin zone are based on a (1x1x5) Monkhorst-Pack three-dimensional grid for cells containing a tube of 150 to 200 atoms along the c axis. Cold smearing is used for the Brillouin zone integration leading to formation energies converged to within 10^{-6} eV. The cell is kept fixed and the atomic positions are relaxed using the conjugate gradient minimization scheme until the magnitude of the forces on all the atoms are smaller than 0.04 Ry/au.

Thermodynamic model
The free energy $F(n,m,T)$ of the system includes three *(n,m)* dependent terms, namely the interfacial energy, the curvature energy, and the configurational entropy contribution. They write:

$$E_{Int}^{(n,m)} = 2\,m\,E_{Int}^A + (n-m)\,E_{Int}^Z$$

$$E_{Curv} = 4\,\alpha\,D_{CNT}^{-2}$$

$$T\,S(n,m) = k_B T\,\ln\frac{n!}{m!(n-m)!}$$

The tube diameter is related to its (n,m) index by the relation
$D_{CNT} = \sqrt{3}\,d_{CC}\,\sqrt{(n^2 + n\,m + m^2)}$, where $d_{CC} = 1.42$ Å is the C-C bond distance. E_{Curv} can then be written:
$$E_{Curv}^{(n,m)} = K\,\frac{(n+m)}{(n^2 + n\,m + m^2)}, \text{ where } K = \frac{4\,\alpha}{3\,d_{CC}^2}$$

Finally, $F(n,m,T)$ writes:
$$F(n,m,T) = 2\,m\,E_{Int}^A + (n-m)\,E_{Int}^Z + K\,\frac{(n+m)}{(n^2 + n\,m + m^2)} - k_B T\,\ln\frac{n!}{m!\,(n-m)!}$$

Transforming the factorials in the entropy term by using Stirling formula would be approximate and useful only to search for an analytical solution at non-zero temperature. For each set of $(T, E_{Int}^A, E_{Int}^Z)$, the chirality *(n,m)* of the most stable SWNT is obtained by minimizing the free energy with respect to *n* and *m*. This minimization is performed numerically in a straightforward way, leading to the results at non-zero temperature presented in the body of the paper. For the sake of completeness, and for a better physical insight, an analytical solution can be developed, exact for ground states, but very approximate at non-zero temperature. The latter is not included here.

Analytical solution for ground states
To minimize the energy at zero Kelvin, it is convenient, in a first step, to consider n and $c = \frac{m}{n}$ as continuous variables, with $0 \le c \le 1$. The free energy becomes

$$F(n, c, T = 0) = n\,\tilde{E}(c) + \frac{1}{n}\,\tilde{K}(c)$$

with:

$\tilde{E}(c) = 2\,c\,E_{Int}^{A} + (1 - c)E_{Int}^{Z}$, and $E_{Int}^{A}, E_{Int}^{Z} > 0$

$\tilde{K}(c) = K\,\frac{1+c}{(1+c+c^2)}$, and $K > 0$

We omit $T = 0$ and now have to minimize $F(n, c)$ with respect to n and c. From $\frac{\partial F}{\partial n} = 0$, we obtain $n^2 = \frac{\tilde{K}(c)}{\tilde{E}(c)}$, hence:

$$F(n(c), c) = 2\sqrt{\tilde{E}(c)\tilde{K}(c)}$$

Minimization of this equation with respect to c then gives:

$$\frac{d\tilde{E}(c)}{dc}\,\tilde{K}(c) + \tilde{E}(c)\,\frac{d\tilde{K}(c)}{dc} = 0$$

Somewhat lengthy calculations show that, for $0 \leq c \leq 1$, the above equation has a solution only for $\frac{1}{2} < \frac{E_{Int}^{A}}{E_{Int}^{Z}} < 1$, in which case the unique solution is not a minimum. In fact, $F(n, c, T = 0)$ is a surface with a downward facing concavity. Minima of $F(c)$ are either obtained for $c = 0$ (zigzag) or $c = 1$ (armchair). This corresponds to a phase separation between two different domains, separated by a line $E_{Int}^{Z} = \frac{4}{3}\,E_{Int}^{A}$.

We now consider n and m as discrete quantities. As a result, two integers n_m and $n_m + 1$ can be defined as $n_m < \sqrt{\frac{\tilde{K}(c)}{\tilde{E}(c)}} < n_m + 1$, where $\sqrt{\frac{\tilde{K}(c)}{\tilde{E}(c)}}$ is the real minimum of the continuous function F. A two-phase coexistence is then observed when $F(n_m, c, T = 0) = F(n_m + 1, c, T = 0)$. For $c = 0$ and $c = 1$ this leads to vertical lines separated by $\frac{K}{n(n+1)}$ and horizontal lines separated by $\frac{K}{3n(n+1)}$, respectively, as presented in Fig. 3-A of the main text.
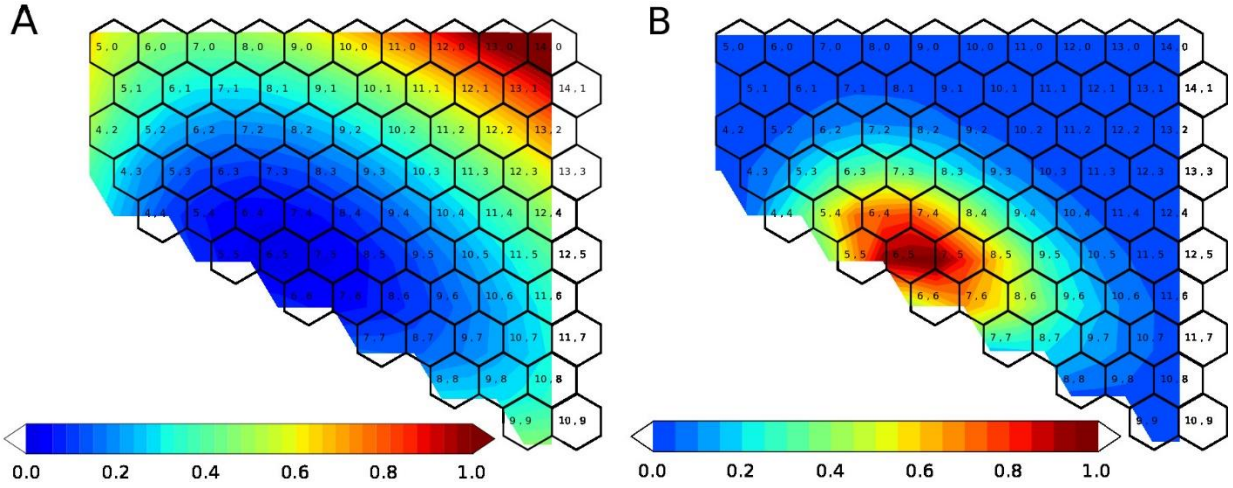
Figure S1 – Probability distribution of chiralities. A : Example of (n,m) dependent contribution to the free energy $F(n, m)$, calculated for $E^Z_{Int} = 250$ meV / bond, $E^A_{Int} = 150$ meV / bond and T = 973 K. **B** : Corresponding $P(n, m)$ probability distribution of chiralities. The minimum of $F(n, m)$ is set to zero, hence the maximum of $P(n, m)$, obtained for the (6,5) chirality in this example, is equal to 1. The neighboring chiralities, such as (7,4) have a probability around 0.6, while second nearest ones, such as (7,3), have probabilities around 0.30.
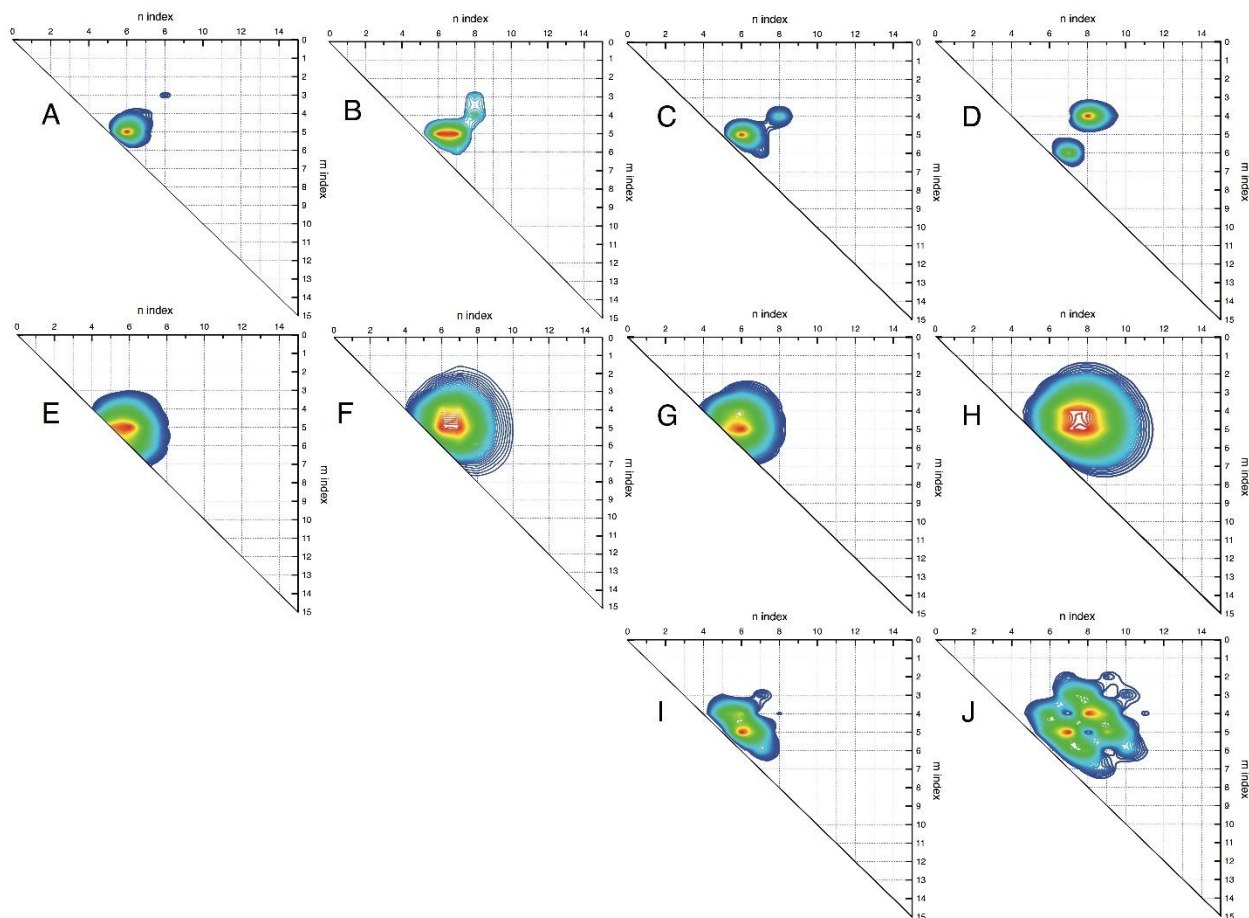
Figure S2 – Comparison with experimental chiral distributions. Interfacial energies are fitted against experimentally determined chiral distributions (A, B, C, D), resulting in calculated distributions (E, F, G, H). Distributions are displayed as contour plots.

A: Electron Diffraction measurement by M. He *et al. (32)* at T = 773 K, and **E**: fitted distribution, obtained for $E_{Int}^Z = \mathbf{0.285}$ eV/bond, $E_{Int}^A = \mathbf{0.163}$ eV/bond.

B: Photoluminescence assignment by Bachilo *et al. (33)* at 1023 K, and **F**: fitted distribution, obtained for $E_{Int}^Z = \mathbf{0.262}$ eV/bond, $E_{Int}^A = \mathbf{0.156}$ eV/bond.

C: Photoluminescence assignment by Li *et al. (24)* at 873 K, and **G**: fitted distribution, obtained for $E_{Int}^Z = \mathbf{0.290}$ eV/bond, $E_{Int}^A = \mathbf{0.175}$ eV/bond. **I**: fitted distribution, plotted without metallic tubes, to better compare with **C**.

D: Photoluminescence assignment by Li *et al.* (*24*) at 1123 K, and **H**: fitted distribution, obtained for $E_{Int}^Z = \mathbf{0.222}$ eV/bond, $E_{Int}^A = \mathbf{0.142}$ eV/bond. **J**: fitted distribution, plotted without metallic tubes, to better compare with **D**.

By construction, our simple two-parameter model produces unimodal distributions, that cannot properly account for scattered experimental chiral distributions, as displayed in **C**, **D**. In such a case the fit results in a flattened and broader distribution. The agreement is somewhat better, when metallic tubes, that don't appear in photoluminescence experiments, are withdrawn from the fitted distributions. We also note that the photoluminescence efficiency, and hence the quantitative evaluation of the chiral distributions, depends on the optical cross section and on the quantum

yield. Both are sensitive to the nanotube chirality *(34, 35)* and to its environment (solvent, surfactant, etc).
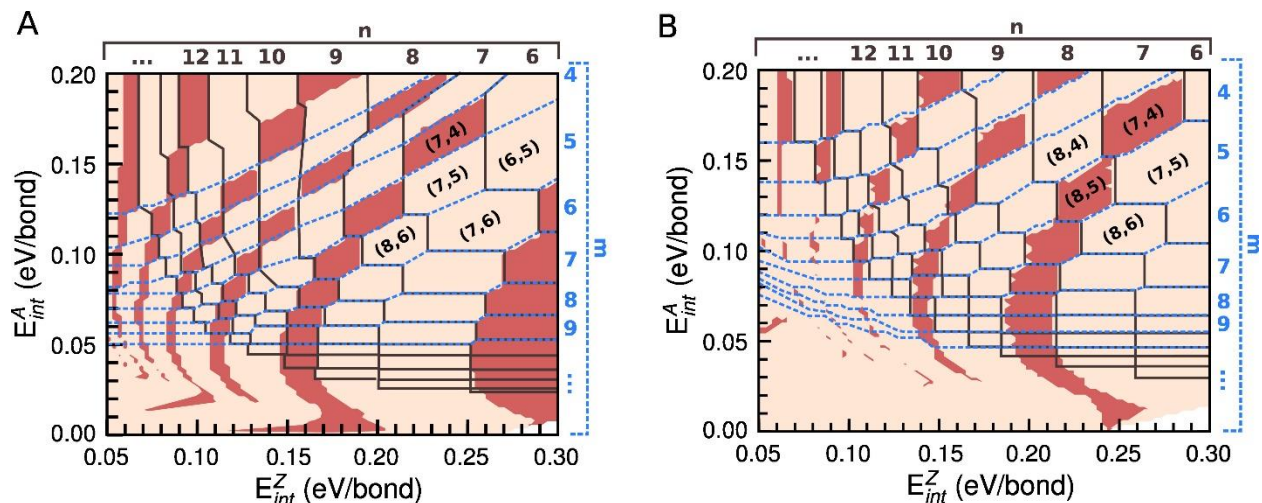
Figure S3 – A) Chirality map at 1000 K. Iso-n (resp. iso-m) values are delimited by full black (resp. dashed blue) lines. Metallic tubes, for which *(n-m)* is a multiple of 3, are shown in brick red, and semi-conducting ones are flesh-colored. The parameter space for armchair (metallic) and *(n, n-1)* and *(n, n-2)* (semi-conducting) tubes is larger than for other chiralities. **B)** Chirality map at 1400 K.

Movie S1.

Movie showing the temperature dependence of the structural maps. As in Figs. S3-A and -B, metallic tubes appear as brick-red, semiconducting ones are in flesh-color. Up to 80 K, only armchair and zigzag tubes are stable, while chiral tubes start to show up at 100 K, in the lower left corner of the map, corresponding to small interfacial energies, hence larger diameter tubes that display a larger configurational entropy. The chiral tubes stability domain then gradually expands along the $E_{Int}^Z = \frac{4}{3} E_{Int}^A$ line. We note that the stability range of armchair and close to armchair domains, *(n, n-1)* and *(n, n-2),* expands faster than the others with increasing temperature. Specific chiral indexes are not displayed in the video, but can be easily identified by comparison with Figs. S3-A and S3-B.

Data S1. (separate file)

Computer codes (Fortran90 and Python) performing the minimization of the free energy $F(n, m)$ for different values of the parameters $(T, E_{Int}^A, E_{Int}^Z)$, and enabling the computation of structural maps are available. Calculating the domain boundaries, by searching points where the free energy difference between two competing phases becomes zero, takes a few minutes with the Fortran code (Chirality_Maps.f90) on a standard workstation, but the identification and coloring of metallic and semi-conducting domains, done in Chiral_Maps.py, is much longer (about 100 minutes per image).

Data S2.

The experimental and fitted data presented in Fig. S2, are displayed below. Each set of experimental data appears as 4 columns: n value, m value, experimental abundance (in italics), fit with our model. The maxima are highlighted in bold. A, E, B, F, C, G and D, H refer to the identifications in Fig. S2.

n	m	*A*	E	n	m	*B*	F	n	m	*C*	G
5	4	*0.00*	0.23	5	4	*0.00*	0.12	4	4	*0.00*	0.09
5	5	*0.00*	0.49	5	5	*0.00*	0.13	5	3	*0.00*	0.08
6	3	*0.00*	0.06	6	3	*0.00*	0.09	5	4	*0.00*	0.33
6	4	*0.09*	0.28	6	4	*0.00*	0.23	5	5	*0.00*	0.43
6	**5**	***0.56***	**0.56**	6	5	*0.28*	0.28	6	3	*0.00*	0.15
6	6	*0.00*	0.38	6	6	*0.00*	0.12	6	4	*0.00*	0.41
7	3	*0.00*	0.05	7	3	*0.00*	0.11	**6**	**5**	***0.54***	**0.54**
7	4	*0.09*	0.14	7	4	*0.00*	0.22	6	6	*0.00*	0.25
7	5	*0.09*	0.26	**7**	**5**	***0.28***	**0.28**	7	3	*0.00*	0.11
7	6	*0.04*	0.23	7	6	*0.09*	0.18	7	4	*0.00*	0.23
7	7	*0.00*	0.08	8	3	*0.11*	0.07	7	5	*0.12*	0.30
8	4	*0.02*	0.04	8	4	*0.14*	0.13	7	6	*0.12*	0.19
8	5	*0.00*	0.07	8	5	*0.00*	0.17	7	7	*0.00*	0.05
8	6	*0.00*	0.07	8	6	*0.00*	0.12	8	4	*0.22*	0.08
8	7	*0.00*	0.03	8	7	*0.00*	0.05	8	5	*0.00*	0.09

n	m	D	H
5	4	0.00	0.09
5	5	0.00	0.07
6	3	0.00	0.14
6	4	0.00	0.27
6	5	0.06	0.27
6	6	0.00	0.10
7	3	0.00	0.25
7	4	0.00	0.44
7	5	0.00	0.45
7	6	0.33	0.24
7	7	0.00	0.05
8	2	0.00	0.11
8	3	0.00	0.27
8	**4**	**0.46**	**0.44**
8	5	0.00	0.46
8	6	0.00	0.30
8	7	0.00	0.10
9	2	0.00	0.09
9	3	0.00	0.20
9	4	0.15	0.31
9	5	0.00	0.34
9	6	0.00	0.24
9	7	0.00	0.11
10	2	0.00	0.05
10	3	0.00	0.10
10	4	0.00	0.17
10	5	0.00	0.19
10	6	0.00	0.15
10	7	0.00	0.08
11	4	0.00	0.07
11	5	0.00	0.08
11	6	0.00	0.07

References and Notes

1. N. Behabtu, C. C. Young, D. E. Tsentalovich, O. Kleinerman, X. Wang, A. W. K. Ma, E. A. Bengio, R. F. ter Waarbeek, J. J. de Jong, R. E. Hoogerwerf, S. B. Fairchild, J. B. Ferguson, B. Maruyama, J. Kono, Y. Talmon, Y. Cohen, M. J. Otto, M. Pasquali, Strong, light, multifunctional fibers of carbon nanotubes with ultrahigh conductivity. *Science* **339**, 182–186 (2013). doi:10.1126/science.1228061 Medline

2. A. D. Franklin, The road to carbon nanotube transistors. *Nature* **498**, 443–444 (2013). [doi:10.1038/498443a](doi:10.1038/498443a) Medline

3. Q. Cao, S.-J. Han, J. Tersoff, A. D. Franklin, Y. Zhu, Z. Zhang, G. S. Tulevski, J. Tang, W. Haensch, End-bonded contacts for carbon nanotube transistors with low, size-independent resistance. *Science* **350**, 68–72 (2015). doi:10.1126/science.aac8006 Medline

4. D. Zhong, Z. Zhang, L. Ding, J. Han, M. Xiao, J. Si, L. Xu, C. Qiu, L.-M. Peng, Gigahertz integrated circuits based on carbon nanotube films. *Nat. Electron.* **1**, 40–45 (2018). [doi:10.1038/s41928-017-0003-y](doi:10.1038/s41928-017-0003-y)

5. M. M. Shulaker, G. Hills, N. Patil, H. Wei, H.-Y. Chen, H.-S. P. Wong, S. Mitra, Carbon nanotube computer. *Nature* **501**, 526–530 (2013). doi:10.1038/nature12502 Medline

6. M. M. Shulaker, G. Hills, R. S. Park, R. T. Howe, K. Saraswat, H. P. Wong, S. Mitra, Three-dimensional integration of nanotechnologies for computing and data storage on a single chip. *Nature* **547**, 74–78 (2017). doi:10.1038/nature22994 Medline

7. F. Yang, X. Wang, D. Zhang, J. Yang, D. Luo, Z. Xu, J. Wei, J.-Q. Wang, Z. Xu, F. Peng, X. Li, R. Li, Y. Li, M. Li, X. Bai, F. Ding, Y. Li, Chirality-specific growth of single-walled carbon nanotubes on solid alloy catalysts. *Nature* **510**, 522–524 (2014). doi:10.1038/nature13434 Medline

8. M. Li, X. Liu, X. Zhao, F. Yang, X. Wang, Y. Li, Metallic Catalysts for Structure-Controlled Growth of Single-Walled Carbon Nanotubes. *Top. Curr. Chem.* **375**, 29 (2017). [doi:10.1007/s41061-017-0116-9](doi:10.1007/s41061-017-0116-9) Medline

9. S. Zhang, L. Kang, X. Wang, L. Tong, L. Yang, Z. Wang, K. Qi, S. Deng, Q. Li, X. Bai, F. Ding, J. Zhang, Arrays of horizontal carbon nanotubes of controlled chirality grown using designed catalysts. *Nature* **543**, 234–238 (2017). doi:10.1038/nature21051 Medline

10. A. A. Puretzky, D. B. Geohegan, S. Jesse, I. N. Ivanov, G. Eres, In situ measurements and modeling of carbon nanotube array growth kinetics during chemical vapor deposition. *Appl. Phys. A* **81**, 223–240 (2005). [doi:10.1007/s00339-005-3256-7](doi:10.1007/s00339-005-3256-7)

11. F. Ding, A. R. Harutyunyan, B. I. Yakobson, Dislocation theory of chirality-controlled nanotube growth. *Proc. Natl. Acad. Sci. U.S.A.* **106**, 2506–2509 (2009). doi:10.1073/pnas.0811946106 Medline

12. V. I. Artyukhov, E. S. Penev, B. I. Yakobson, Why nanotubes grow chiral. *Nat. Commun.* **5**, 4892 (2014). doi:10.1038/ncomms5892 Medline

13. A. J. Page, F. Ding, S. Irle, K. Morokuma, Insights into carbon nanotube and graphene formation mechanisms from molecular simulations: A review. *Rep. Prog. Phys.* **78**, 036501 (2015). [doi:10.1088/0034-4885/78/3/036501](doi:10.1088/0034-4885/78/3/036501) Medline

14. H. Amara, C. Bichara, Modeling the Growth of Single-Wall Carbon Nanotubes. *Top. Curr. Chem.* **375**, 55 (2017). [doi:10.1007/s41061-017-0141-8](doi:10.1007/s41061-017-0141-8) Medline

15. M.-F. C. Fiawoo, A.-M. Bonnot, H. Amara, C. Bichara, J. Thibault-Pénisson, A. Loiseau, Evidence of correlation between catalyst particles and the single-wall carbon nanotube diameter: A first step towards chirality control. *Phys. Rev. Lett.* **108**, 195503 (2012). doi:10.1103/PhysRevLett.108.195503 Medline

16. M. He, Y. Magnin, H. Jiang, H. Amara, E. I. Kauppinen, A. Loiseau, C. Bichara, Growth modes and chiral selectivity of single-walled carbon nanotubes. *Nanoscale* **10**, 6744–6750 (2018). [doi:10.1039/C7NR09539B](doi:10.1039/C7NR09539B) Medline

17. Y. Liu, A. Dobrinsky, B. I. Yakobson, Graphene edge from armchair to zigzag: The origins of nanotube chirality? *Phys. Rev. Lett.* **105**, 235502 (2010). doi:10.1103/PhysRevLett.105.235502 Medline

18. O. Gülseren, T. Yildirim, S. Ciraci, Systematic ab initio study of curvature effects in carbon nanotubes. *Phys. Rev. B* **65**, 153405 (2002). doi:10.1103/PhysRevB.65.153405

19. T. Wassmann, A. Seitsonen, A. M. Saitta, M. Lazzeri, F. Mauri, Structure, Stability, Edge States, and Aromaticity of Graphene Ribbons. *Phys. Rev. Lett.* **101**, 096402 (2008). doi:10.1103/PhysRevLett.101.096402

20. F. Ding, P. Larsson, J. A. Larsson, R. Ahuja, H. Duan, A. Rosén, K. Bolton, The importance of strong carbon-metal adhesion for catalytic nucleation of single-walled carbon nanotubes. *Nano Lett.* **8**, 463–468 (2008). [doi:10.1021/nl072431m](doi:10.1021/nl072431m) Medline

21. A. Börjesson, K. Bolton, First Principles Studies of the Effect of Nickel Carbide Catalyst Composition on Carbon Nanotube Growth. *J. Phys. Chem. C* **114**, 18045–18050 (2010). [doi:10.1021/jp1045707](doi:10.1021/jp1045707)

22. L. Henrard, A. Loiseau, C. Journet, P. Bernier, What is the chirality of singlewall nanotubes produced by arcdischarge? An electron diffraction study. *Synth. Met.* **103**, 2533–2536 (1999). [doi:10.1016/S0379-6779(98)00321-X](doi:10.1016/S0379-6779(98)00321-X)

23. R. M. Sundaram, K. K. K. Koziol, A. H. Windle, Continuous direct spinning of fibers of single-walled carbon nanotubes with metallic chirality. *Adv. Mater.* **23**, 5064–5068 (2011). doi:10.1002/adma.201102754 Medline

24. X. Li, X. Tu, S. Zaric, K. Welsher, W. S. Seo, W. Zhao, H. Dai, Selective synthesis combined with chemical separation of single-walled carbon nanotubes for chirality selection. *J. Am. Chem. Soc.* **129**, 15770–15771 (2007). [doi:10.1021/ja077886s](doi:10.1021/ja077886s) Medline

25. H. Wang, B. Wang, X.-Y. Quek, L. Wei, J. Zhao, L.-J. Li, M. B. Chan-Park, Y. Yang, Y. Chen, Selective synthesis of (9,8) single walled carbon nanotubes on cobalt incorporated TUD-1 catalysts. *J. Am. Chem. Soc.* **132**, 16747–16749 (2010). [doi:10.1021/ja106937y](doi:10.1021/ja106937y) Medline

26. M. He, A. I. Chernov, P. V. Fedotov, E. D. Obraztsova, J. Sainio, E. Rikkinen, H. Jiang, Z. Zhu, Y. Tian, E. I. Kauppinen, M. Niemelä, A. O. I. Krause, Predominant (6,5) single-walled carbon nanotube growth on a copper-promoted iron catalyst. *J. Am. Chem. Soc.* **132**, 13994–13996 (2010). [doi:10.1021/ja106609y](doi:10.1021/ja106609y) Medline

27. M. Fouquet, B. C. Bayer, S. Esconjauregui, R. Blume, J. H. Warner, S. Hofmann, R. Schlögl, C. Thomsen, J. Robertson, Highly chiral-selective growth of single-walled carbon nanotubes with a simple monometallic Co catalyst. *Phys. Rev. B* **85**, 235411 (2012). doi:10.1103/PhysRevB.85.235411

28. F. Silvearv, P. Larsson, S. Jones, R. Ahuja, J. A. Larsson, Establishing the Most Favorable Metal-Carbon Bond Strength for Carbon Nanotube Catalysts. *J. Mater. Chem. C* **3**, 3422–3427 (2015). doi:10.1039/C5TC00143A

29. P. Giannozzi, S. Baroni, N. Bonini, M. Calandra, R. Car, C. Cavazzoni, D. Ceresoli, G. L. Chiarotti, M. Cococcioni, I. Dabo, A. Dal Corso, S. de Gironcoli, S. Fabris, G. Fratesi, R. Gebauer, U. Gerstmann, C. Gougoussis, A. Kokalj, M. Lazzeri, L. Martin-Samos, N. Marzari, F. Mauri, R. Mazzarello, S. Paolini, A. Pasquarello, L. Paulatto, C. Sbraccia, S. Scandolo, G. Sclauzero, A. P. Seitsonen, A. Smogunov, P. Umari, R. M. Wentzcovitch, QUANTUM ESPRESSO: A modular and open-source software project for quantum simulations of materials. *J. Phys. Condens. Matter* **21**, 395502 (2009). doi:10.1088/0953-8984/21/39/395502 Medline

30. P. E. Blöchl, Projector augmented-wave method. *Phys. Rev. B* **50**, 17953–17979 (1994). doi:10.1103/PhysRevB.50.17953 Medline

31. J. P. Perdew, K. Burke, M. Ernzerhof, Generalized Gradient Approximation Made Simple. *Phys. Rev. Lett.* **77**, 3865–3868 (1996). doi:10.1103/PhysRevLett.77.3865 Medline

32. M. He, H. Jiang, B. Liu, P. V. Fedotov, A. I. Chernov, E. D. Obraztsova, F. Cavalca, J. B. Wagner, T. W. Hansen, I. V. Anoshkin, E. A. Obraztsova, A. V. Belkin, E. Sairanen, A. G. Nasibulin, J. Lehtonen, E. I. Kauppinen, Chiral-selective growth of single-walled carbon nanotubes on lattice-mismatched epitaxial cobalt nanoparticles. *Sci. Rep.* **3**, 1460 (2013). doi:10.1038/srep01460 Medline

33. S. M. Bachilo, L. Balzano, J. E. Herrera, F. Pompeo, D. E. Resasco, R. B. Weisman, Narrow (n,m)-distribution of single-walled carbon nanotubes grown using a solid supported catalyst. *J. Am. Chem. Soc.* **125**, 11186–11187 (2003). doi:10.1021/ja036622c Medline

34. S. Reich, C. Thomsen, J. Robertson, Exciton resonances quench the photoluminescence of zigzag carbon nanotubes. *Phys. Rev. Lett.* **95**, 077402 (2005). doi:10.1103/PhysRevLett.95.077402 Medline

35. Y. Oyama, R. Saito, K. Sato, J. Jiang, G. G. Samsonidze, A. Grüneis, Y. Miyauchi, S. Maruyama, A. Jorio, G. Dresselhaus, M. S. Dresselhaus, Photoluminescence intensity of single-wall carbon nanotubes. *Carbon* **44**, 873–879 (2006). doi:10.1016/j.carbon.2005.10.024